Research Article

Performance of poly sulfonamide/nano-silica composite for adsorption of thorium ions from sulfate solution

Mohamed F. Cheira[1]

Received: 4 December 2019 / Accepted: 10 February 2020 / Published online: 13 February 2020

Abstract
A new composite of poly sulfonamide/nano-silica composite (PSA/silica) was synthesized from the polymerization of sulfonamide in the presence of the prepared nano-silica. The prepared nano-silica, poly sulphonamide (PSA), and PSA/silica composites were utilized for Th(IV) adsorption from sulfate solution. These composites described by XRD, surface area analysis, SEM–EDX, and FT-IR techniques. The influence parameters on the Th(IV) adsorption were pH solution, ionic strength, contact time, adsorbent dose, Th(IV) concentration, and temperature besides the coexisting ions. At best parameters (pH4, 0.1 g adsorbent amount, and 45 min contact time), 200 mg/L Th(IV) ions were quantitatively adsorbed from 100 mL solution. The maximum uptake capacities of the nano-silica, PSA, and PSA/silica composites attained 122, 75, and 197 mg/g at 298 K. From the kinetic and equilibrium data were found to the adsorption processes of three composites fitted well with kinetic model of pseudo-second-order and Langmuir adsorption isotherm model. Thermodynamic studies resulted that negative values for $\Delta H°$ indicated an exothermic while positive values $\Delta S°$ showed random behavior for Th(IV) adsorption, while negative values of $\Delta G°$ indicated spontaneous Th(IV) adsorption. The maximum Th(IV) desorption from the loaded adsorbents performed by 0.1 M/L HCl.

Keywords Separation · Silica · Polysulfonamide · Thorium · Equilibrium · desorption

1 Introduction

The increase in industrial applications and nuclear activities over the earlier decades were improved significantly through the evolution of the suitable metal ions separation techniques. However, the challenge of energy deficiencies developing more seriously exceeding and nuclear power was importantly utilized in industrial productions and living. Thorium ions have attracted much knowledge as an essential nuclear fuel [1]. Th(IV) is a highly toxic and radioactive element that exists naturally in a tetravalent valence. Thorium ions have been broadly used in the reactors of nuclear power and refractory material into tubes, rods, crucibles, etc., anti-reflection cover in making ceramics optics, the additive for unique glass, gas lantern mantles, metal alloys for some aerospace manufacturing and aeronautics components, welding alloys, catalyst in chemistry and fuel for generating nuclear energy [2, 3].

A set of technologies were forerun to separate thorium ions from its solutions, and these methods were chemical precipitation [4], ion exchange [5, 6], liquid–liquid extraction [7–9], and adsorption [10–12]. Amongst these techniques, adsorptions are typical extensively utilized for separating heavy and radioactive metal ions on laboratory and industrial scales, because this method is low-cost, environmentally compatible and very efficient [13]. Recently, various efforts were applied to synthesize unique materials to extract Th(IV) from its solution. Several adsorbents materials employed for the adsorption of thorium ions including polymers, clay, metal oxides and poly materials/metal oxides [14–17]. Nevertheless, low adsorption potentials, inadequate adsorption states, and

✉ Mohamed F. Cheira, mf.farid2008@yahoo.com | [1]Nuclear Materials Authority, El Maadi, Cairo, Egypt.

SN Applied Sciences (2020) 2:398 | https://doi.org/10.1007/s42452-020-2221-6

inconvenient separation reduced their practical objectives. Therefore, it is essential to manufacture innovative adsorbents that have excellent adsorption capacities for extensive applications in thorium ions separation.

In recent years, metal oxides nanoparticles created noteworthy consideration because of their physical and chemical stability, nontoxicity, unique substantial specific surface area, and uniform pore structure [18]. There are Nano silicon dioxide prepared for the adsorption of Th(IV) from aqueous solution [19]. Thorium ions removed from waste solutions using the synthesized nanoporous ZnO while nano tin oxide utilized for Th(IV) and U(VI) elimination from aqueous solutions [20, 21]. Thorium ions adsorption on nanoporous silicate was also reported from chloride solution [22].

Throughout the earlier few decades, nano metal oxides adsorbents were combined with polymers that had held great potential in thorium(IV) recovery. Fumed silica was prepared using mechanochemical activation of wetted nano-silica, it was used as a matrix for the preparation of a composite with glucose and by the carbonization of glucose gave weakly porous char nanoparticles [23], the electrical and physical characteristics of nano-silica were obtained in aqueous solution [24]. Nano-silica was supported with metal oxides (M_xO_y) to form inorganic nanocomposites [25]. However, polymers were characterized by the efficient, accessible, low-cost and extremely versatile strategy to adsorb metal ions from its solutions due to existing of functional groups in the polymers structures [26–28]. While the adsorption selectivity and capacity for the nano-silica and also polymers individually were still restricted, owing to the lacking active site at the adsorbents surfaces. To solve that problem, silica nanoparticles were immobilized with organic materials such as polyvinyl alcohol that improved their thermal and mechanical properties as well as enhancement adsorption capacity for Th(IV) ions [29].

In order to increase the extent of poly sulphonamides materials adsorption, the adsorption potential of metal ions was studied by the anchored sulfonamide polymers with numerous materials. Sulphonamides include sulfadiazine, sulfamethizole, sulfisoxazole, sulfasalazine, sulfamethoxazole, and numerous high-strength sequences of sulfonamides. The main poly sulfonamides (polymer-SO_2-NH-polymer) have the acidic proton on sulfonamide nitrogen. When poly sulfonamides exposed to sufficiently alkaline solutions, the sulfonamide group became negatively charged due to the removed hydrogen ions. Polysulfonamide (PSA) is a kind of great performance synthetic polymer that has a unique thermal, dielectric, mechanical properties, along with superior chemical resistance [30–33]. After modification of nanoporous silica with sulfonamide derivative has certain advantages for thorium ions removal.

The purpose of the present work was to study the efficiency of the prepared PSA/nano-silica as a new adsorbent for adsorbing thorium ions from sulfate solution. The impact of different laboratory parameters, including pH, ionic strength, contact time, initial Th(IV) concentration, adsorbent amount and temperature, besides adsorption kinetics, isotherm models, and thermodynamics, were studied on nano-silica, PSA, and PSA/nano-silica composites. Besides, the properties of reusability and selectivity of PSA/nano-silica were also investigated.

2 Materials and methods

2.1 Instruments and materials

A double-beam UV/Vis spectrophotometer model 160A, Shimadzu utilized for determining thorium(IV) by Thoron I as an indicator [34]. Inductively-coupled-plasma-optical-emission spectrometry (Leeman Labs USA) also used for Th(IV) and trace metals ions measurements. The Fourier transform-infrared spectrometer (FTIR, Thermo Scientific USA) utilized to describe the major functional groups of the synthesized adsorbents and the Th(IV) loaded adsorbents. Scanning electron microscopy technique (SEM, Jeol-JSM-5600-LV) provided by the Oxford Instruments 6587 EDX microanalysis detector (Japan) was used for the morphological properties of the studied adsorbents. The average pore size and specific surface area of all solid adsorbents were evaluated with the Brunauer–Emmett–Teller (BET) by N_2 adsorption/desorption isotherms. X-Ray Diffraction technique (XRD) was done to know the identified minerals.

A stock solution of thorium ions (1000 mg/L) was prepared via the dissolving of 5.07 g thorium nitrate hexahydrate (Fluka, 98%) in 200 mL of 5 M sulfuric acid (BDH, 98%) and then complete to 2000 mL with distilled water. The stock solution was utilized to assess the relevant factors of Th(IV) adsorption. All the chemicals and reagents employed in all different parts of this work are analytical grade. All solvents were directly utilized as purchased without extra purification for the preparation of the adsorbents. Tetraethyl orthosilicate (TEOS, Aldrich, 99%), cetyltrimethylammonium bromide (CTAB, Fulka, 98%), ethanol (BDH), 2-methyl pyridine (BDH, 99%), dimethylacetamide (DMAc, Merck, 99%), 4, 4′ di-amino diphenyl sulfone (APS, Merck, 99%) and terephthaloyl chloride (Fulka, 99%) were utilized as received.

2.2 Synthesis of nano-silica

Mesoporous spherical nano-silica was obtained by the hydrothermal method [35]. The cetyltrimethylammonium bromide (CTAB) surfactant (2 g) dissolved in 800 mL deionized water containing 1 M NaOH (10 mL) and ethanol (100 mL), with agitating at 80 °C to obtain a clear solution. Then, 11.7 mL tetraethyl-orthosilicate (TEOS) added to the fine solution with vigorous stirring. After 2 h of continuous stirring at 80 °C, the white precipitate derived through filtration, and it washed with ethanol at least three times, then the precipitate dried for 12 h and 60 °C. The powder was calcined for 4.5 h and 600 °C to eliminate the surfactant, the obtained fine powder was nano-silica that analyzed by spectrophotometric technique.

2.3 Preparation of PSA

Polysulfonamide was prepared [36–39] by dissolving of 0.1 M/L of 4, 4′ diamino diphenyl sulfone (APS) in 120 mL of N, N dimethylacetamide (DMAc) and kept stirring the mixture in the three-necked flask, till the solution (APS/DMAc) was dissolved. The system was cooled to − 17 °C using a bath of a mixture of acetone and liquid nitrogen. Under the low temperature, 0.1 M/L of terphthaloyl chloride was added into the mixture solution with stirring. After total diacid chloride was dissolved, the mixture was agitated at 25 °C, and 45 min. Then, 0.2 M/L of 2-methylpyridine (as the acid acceptor) was added to the solution to neutralize and pick up whole hydrochloric acid produced. If the acid acceptor was not sufficiently reactive, in the medium to capture full hydrochloric acid produced, contamination of the system and side reactions occurred, avoiding high molecular weight, and the solution was further agitated for 3.5 h. The polymer was isolated via pouring the solution with stirring inside a beaker holding 500 mL of cold water and collected by filtration. The outcome was washed by water and methanol, then dried against the vacuum oven.

2.4 Preparation of PSA/silica nanocomposite

A certain quantity of nano SiO_2 (6 g) was dispersed in 120 mL of DMAc, and the mixture (DMAc/SiO_2) was added into a mixture of APS/DMAc, The above-mentioned the way of preparation was the same as that of PSA. Then, 0.1 M/L of terephthaloyl chloride was added at a low temperature (below 0 °C) for 4 h. Then antacid was put into the mixture to adjust the solution pH below 7. The mixed solution was coated on the fine glass substrate and dried for 8 h and 80 °C to obtain PSA/SiO_2 nanocomposite.

2.5 Adsorption investigations

A set of adsorption experiments carried out by batch adsorption mode, at 0.1 g adsorbent, 100 mL of solution assaying 200 mg/L of the initial Th(IV) concentration in stoppered flasks, at different pH values and the solution was placed at a different temperatures (25–55 °C) on the motorized shaker at 100 rpm until the equilibrium time. For determining the pH impact on the adsorption capacities of nano-silica, PSA, and PSA/SiO_2 adsorbents, various tests were done at varying pH values, ranging from 1–7 for thorium ions solution. The pH of solutions was adjusted using 0.2 M/L NaOH and/or H_2SO_4 solutions. The ionic strength impact studied for the range of 0–0.1 M/L by adding different background salts (NaCl, KCl, and $MgCl_2$), and then the solutions were shaken at 25 °C. The contact time was studied in the range 5–120 min and other parameters were kept constant while the adsorbents doses were done in the range 20–200 mg. The kinetic adsorption tests were also made by accretion of 0.1 g adsorbent within a series of stoppered flasks having 100 mL of 200 mg/L of thorium ions solution at 25 °C during the time range 5–120 min. Also, adsorption isotherms were taken into consideration at three adsorbents in various concentrations of thorium ions solutions from 25 to 800 mg/L within adsorption system. The supernatants were filtered and the concentrations of Th(IV) in the solutions were measured before and after the establishment of equilibrium. The adsorption capacity q_e (mg/g), and adsorption efficiency E (%) could design by the mass balance equations:

$$q_e = (C_i - C_f) \times \frac{V}{W} \quad (1)$$

$$E, \% = \frac{C_i - C_f}{C_i} \times 100 \quad (2)$$

where C_f and C_i are final and initial Th(IV) concentrations (mg/L) in solution, respectively, and V is the liquid volume (L), and W denotes the adsorbent amount (g).

2.6 Desorption investigations

The desorption tests were applied by different concentrations HCl to desorb Th(IV) from the loaded adsorbents. Each operation was achieved by agitating 2 g of Th(IV) loaded adsorbent by 50 mL varying concentrations of HCl within 60 min contact time at ambient temperature.

3 Results and discussion

3.1 Description of adsorbents

3.1.1 XRD analysis

XRD diffraction patterns of the nano-SiO_2, PSA, and PSA/SiO_2 were achieved in Fig. 1. The diffraction spectrum of the nano-SiO_2 exhibited two major broad peaks at $2\theta = 24°$ and a shoulder at $2\theta = 43°$ (JCPDS card 16-0380). The first peak at $2\theta = 24°$, that is at a significantly high point in Fig. 1a, exhibited the anisotropic crystallographic nature of the silica particles and the manner the particles are alongside one another [40]. The size of the nano-SiO_2 crystalline was evaluated from the Debye–Scherrer equation ($d = k\lambda/\beta \cos\theta$) [41] where d is the average diameter of nanoparticles (nm), k is the Scherrer constant ($k = 0.89$), θ is the diffraction angle, λ is the wavelength of X-ray radiation (1.542 nm), and β is the full width at half maximum of X-ray diffraction peaks. The crystalline sizes of SiO_2 particles were about 20 nm (using the (101) index at $2\theta = 24°$).

As exposed in Fig. 1c, a broad peak with low intensity at $2\theta = 20°$ was characteristic of a PSA polymer. The diffraction spectra of PSA/SiO_2 were presented in Fig. 1b. Compared with that of the nano-SiO_2 and the PSA polymer, the peak at $2\theta = 24°$ was moderately low, while the peak position and peak shape at $2\theta = 43°$ were not altered, and the broad peak of nano-SiO_2 fully overlapped with the peak of PSA at $2\theta = 20°$. Also, in the XRD pattern of PSA/SiO_2 composite, there were new peaks at $2\theta = 62 \sim 68°$ that may be due to the surface electrostatic interaction between nano-silica with PSA to form a new composite (PSA/SiO_2) (Fig. 1b). Therefore, the combination of PSA and nano-SiO_2 might take place on the silica surface without changing the microstructure of the nano-SiO_2.

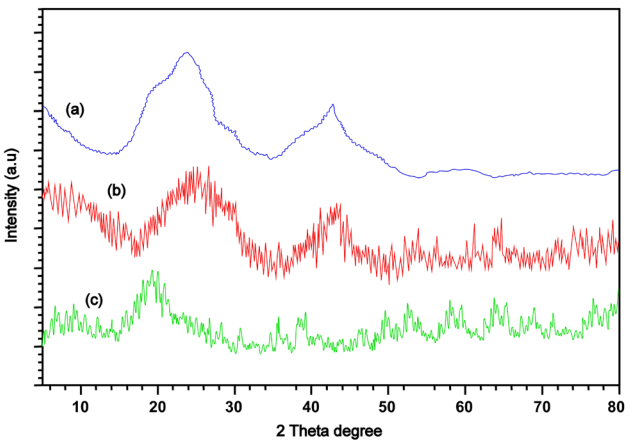

Fig. 1 XRD designs of **a** nano-SiO_2, **b** PSA/SiO_2 composite, and **c** PSA polymer

3.1.2 SEM studies

The SEM was also utilized to probe the surface, and internal structures change of nano-SiO_2, PSA, and PAS/SiO_2 before and after Th(IV) adsorption ions as displayed in Fig. 2. Nano-SiO_2 has exhibited a typical fine shape with a fine rough structure and low density. However, its fine shape increased after cross-linking with the PSA and also after adsorption with thorium ions as expected. The morphology of nano-SiO_2 revealed that the SiO_2 skeleton was constituted of small spherical particles with a small diameter, and they interconnected each other, leading to interstitial space and the rough surface of the SiO_2 (Fig. 2a). While the surface of PSA was smoothly accompanied by several cavities as exposed in Fig. 2c. The development of the interstitial space and the interconnecting structure were possibly due to the collection of the small molecules SiO_2 particles and the removal of the solvent [38]. As in Fig. 2e, similar to the SiO_2, the morphology of PSA/SiO_2 composite was constructed of aggregates particles and with larger interstitial space structure. However, the PSA/SiO_2 composite had a relatively smooth surface that might have resulted from the covering of the PSA on the SiO_2 surface.

After the adsorption process, SEM images in Fig. 2b, d, f, showed that the cavities or pores were filled, and the surfaces were very smooth, irregular and agglomerate with thorium ions. The reason for the significant difference in the compositions due to the cavities in PSA produced vital adsorption channel and space for Th(IV) ions. In addition, the SEM results reveal that the structure of PSA/SiO_2 created a more extensive surface area for Th(IV) adsorption, which was better than nano-SiO_2 and PSA for its reacted with metal ions by giving larger and wider exposed sites for reaction.

3.1.3 EDX studies

The chemical compositions of nano-SiO_2, PSA, and PAS/SiO_2 before and after Th(IV) adsorption ions were analyzed by EDX elemental analysis, as displayed in Fig. 3. The chemical composition of SiO_2, PSA, and PAS/SiO_2 before adsorption were obtained. From the results in Fig. 3a, only Si (32.14%) and O (67.86%) peaks were presented, and no other peaks are detected. Silicon to oxygen atomic ratio about 1:2 has corresponded with the silica structures that have only SiO_4 tetrahedra, and the 1:2 ratio of SiO_2 requires that each oxygen atom is shared by two tetrahedra in silica [42]. It means that the prepared SiO_2 possesses high purity.

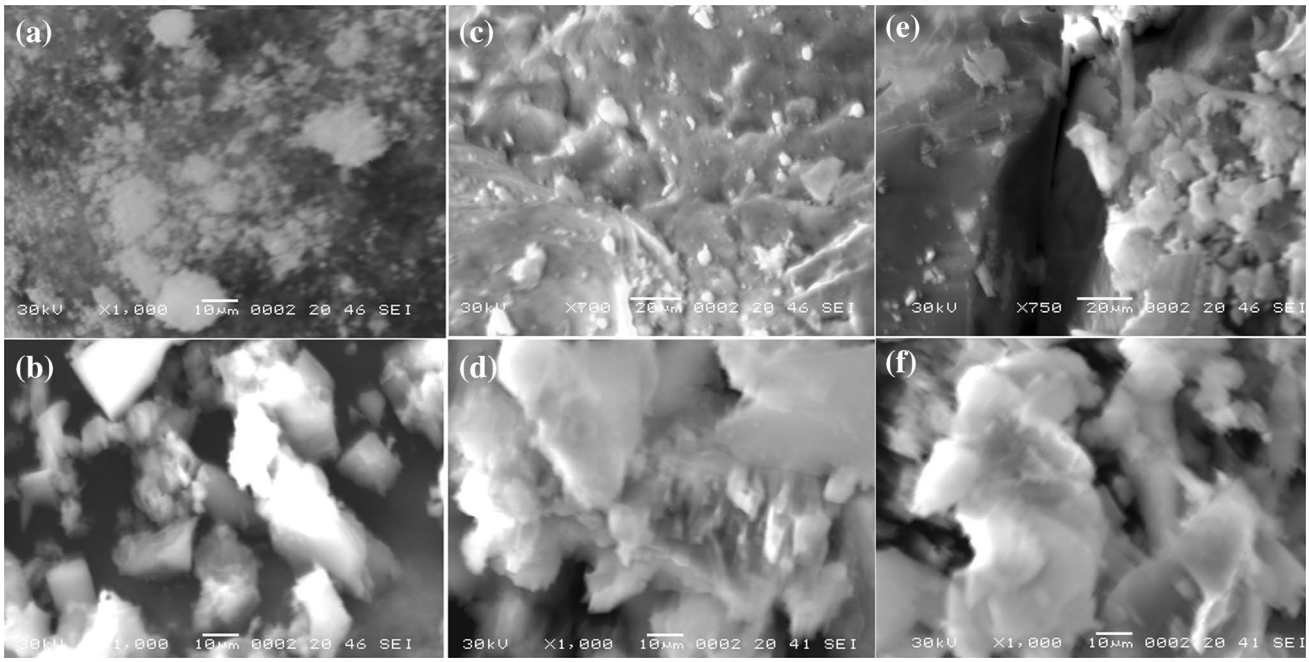

Fig. 2 SEM photographs of **a** nano-SiO_2, **b** Th-loaded SiO_2, **c** PSA, **d** Th-loaded PSA, **e** PSA/SiO_2, and **f** Th-loaded PSA/SiO_2

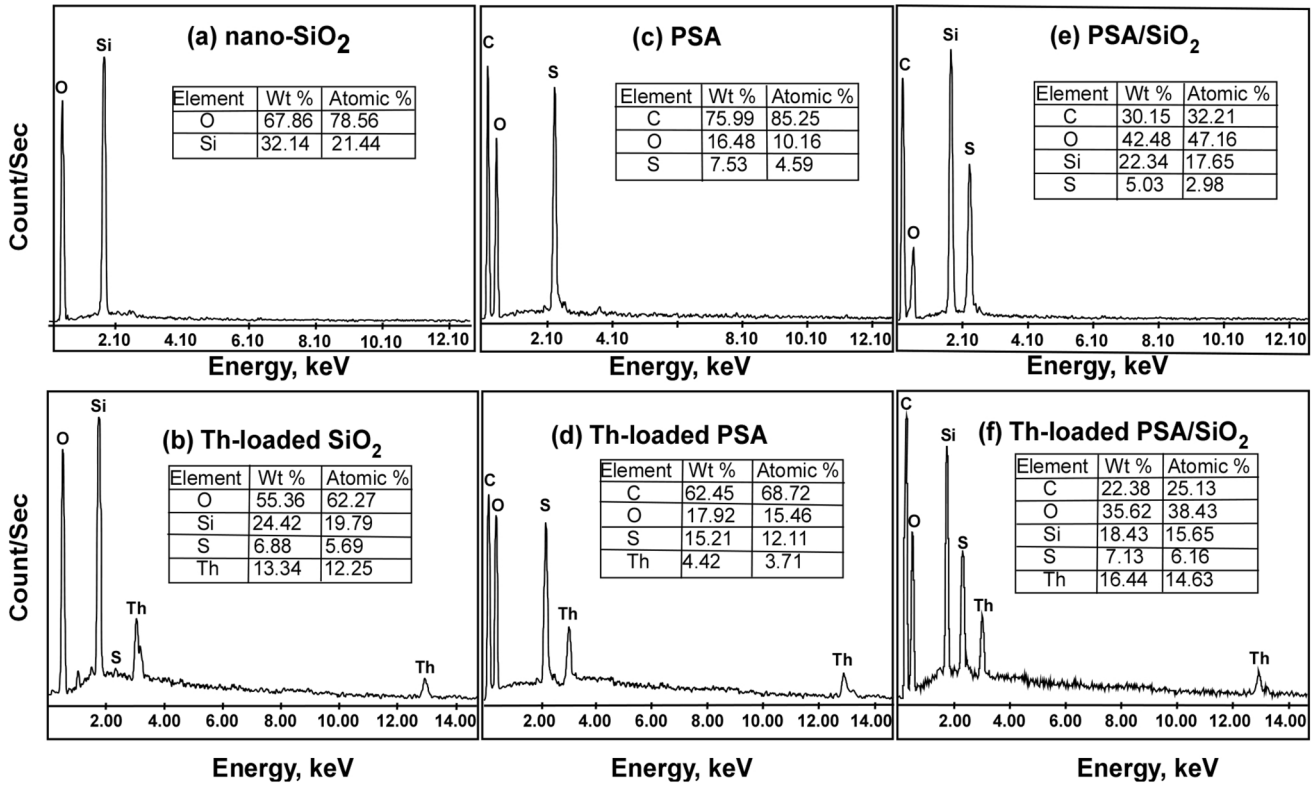

Fig. 3 EDX spectrum of **a** nano-SiO_2, **b** Th-loaded SiO_2, **c** PSA, **d** Th-loaded PSA, **e** PSA/SiO_2, and **f** Th-loaded PSA/SiO_2

Figure 3c expressed that the elemental composition of the PSA was obtained by energy spectrum analysis, it contained C (75.99%), O (16.48%), and S (7.53%) peaks, but in Fig. 3e showed a combination peaks between SiO_2 and PSA composite. These results confirmed that the combination of SiO_2 and PSA occurred to gain PSA/SiO_2 composite. After thorium ions adsorption on the three adsorbents, it could be observed clearly from Fig. 3b, d, f, that were was a distinct peaks of thorium on the three adsorbents spectra. A thorium peak was detected, confirming the adsorption of thorium ions on nano-SiO_2, PSA, and PAS/SiO_2.

3.1.4 Surface analysis

The nitrogen adsorption–desorption analyzer was conducted to evaluate the specific surface area and the pore size of nano-SiO_2, Th-loaded SiO_2, PSA polymer, Th-loaded PSA, PSA/SiO_2, and Th-loaded PSA/SiO_2. Figure 4 shows the nitrogen adsorption–desorption isotherm curves of these materials. The data exhibited that the N_2 isotherm behavior corresponded to type IV of adsorption/desorption isotherm instituted by the IUPAC organization. The isotherms altered clearly after nano-SiO_2 modification with PSA. From the obtained data, the Brunner–Emmet–Teller (BET) surface area of nano-SiO_2, PSA, and PSA/SiO_2 was 50.43, 7.55, and 35.72 m^2/g, respectively. The specific surface area, pore-volume, and pore size of PSA/SiO_2 were significantly between the corresponding values of nano-SiO_2 and PSA, and it could be attributed that nano-SiO_2 adorned PSA pores. The surface area and porosity of the addition of nano-SiO_2 improved the coverage of the organic polymer PSA to trap thorium ions.

The nano-SiO_2 and its adsorption of thorium ions decreased the surface area from 50.43 to 31.15 m^2/g, and pore volume reduced from 0.122 to 0.113 cm^3/g, besides the pore size decreased from 15.57 to 11.27 nm, respectively. The PSA and its trapping of thorium ions decreased the surface areas from 7.55 to 5.36 m^2/g, and pore volume reduced from 0.204 to 0.196 cm^3/g, as well as pore size decreased from 95.34 to 88.25 nm, respectively. In the same way, the PSA/silica and its loaded with thorium ions decreased the surface areas from 35.72 to 22.56 m^2/g, and pore volume decreased from 0.175 to 0.155 cm^3/g, as well as pore size, decreased from 72.24 to 65.21 nm, respectively. From the given data, the surface area, pore size, and pore volume of nano-silica, PSA and PSA/silica decreased after thorium ions adsorption because of pore-blocking with thorium ions. The obtained results revealed that the thorium ions were strongly adsorbed with the PSA/silica more than nano-silica and PSA individually, due to the PSA/silica has more active sites than nano-silica and PSA.

3.1.5 Infrared analysis

The nano-SiO_2, Th-loaded SiO_2, PSA polymer, Th-loaded PSA, PSA/SiO_2, and Th-loaded PSA/SiO_2 were characterized by FT-IR spectroscopy, and the results were displayed in Fig. 5. Before Th(IV) adsorption, in Fig. 5a for the nano-SiO_2, the wide peak at around 3443 cm^{-1} was donated to the O–H stretching vibration band of the nano-SiO_2 and/or adsorbed H_2O molecules upon silica surface, but the vibration band of captured H_2O molecules by silica was detected at 1634 cm^{-1} which could not be completely removed by drying [43]. The predominant band at 1985 cm^{-1} related to the asymmetric vibration band of the siloxane bond Si–O–Si [44]. The presence of peak at 957 cm^{-1} was recognized as the bending vibration of the silanol group (Si–OH). the presence of an absorption band at 798 cm^{-1} was assigned to Si–O–Si stretching vibration band. The vibration band detected at 467 cm^{-1} because of the vibration of the Si–O–Si vibration bond [45].

In Fig. 5c for the poly sulfonamide (PSA) could be seen that strong two peaks at 3285 cm^{-1} and 1673 cm^{-1} were characteristic of –NH and C=O bands of amide groups. The PSA was also characterized by the transmittance of mono-substituted amide linkages (C–N stretch) at 1504 cm^{-1}. The characteristic bands of sulfonamide were seen at 1409 cm^{-1} and 1324 cm^{-1} (fragmented of asymmetrical stretch of –SO_2N–) and 1148 cm^{-1} (symmetrical stretch of -SO_2N-) [46].

In Fig. 5e, the symmetric stretching vibration absorption band of Si–OH was at around 3399 cm^{-1}, and the bands at 465, 804, and 1098 cm^{-1} were assigned to the Si–O cm^{-1}Si stretching vibration absorption bands, which the transmittance correspondingly decreased. The characteristic absorption of sulfonamide groups shifted to 1412, 1331, and 1151 cm^{-1} of the symmetrical stretch of -SO_2N- which suggested that the SiO_2 surface was partially shielded by PSA through acid–base interaction (hydrogen bonds) between nitrogen atom in PSA and silanol group of silica. This finding indicated that SiO_2 and PSA were successfully composed together to form PSA/SiO_2.

After Th(IV) adsorption, the –OH, –NH and C=O stretching vibration bands for the three adsorbents reduced and shifted to redshift with 10–15 cm^{-1}, which may be owing to the linkage of Th(IV) to the three adsorbents surfaces. Moreover, sharp peaks were detected at 1389 cm^{-1} and 1051 cm^{-1} for Th-loaded silica (Fig. 5b), and at 1381 cm^{-1} and 1050 cm^{-1} for Th-loaded PSA (Fig. 5d), as well as at 1391 cm^{-1} and 1043 cm^{-1} for Th-loaded PSA/silica (Fig. 5f), these peaks corresponded to the Th–O vibration band of thorium ions, providing direct evidence for Th^{4+} adsorption on the three adsorbents [47]. These results indicated the adsorption of thorium ions on the nano-silica, PSA, and PSA/silica surfaces.

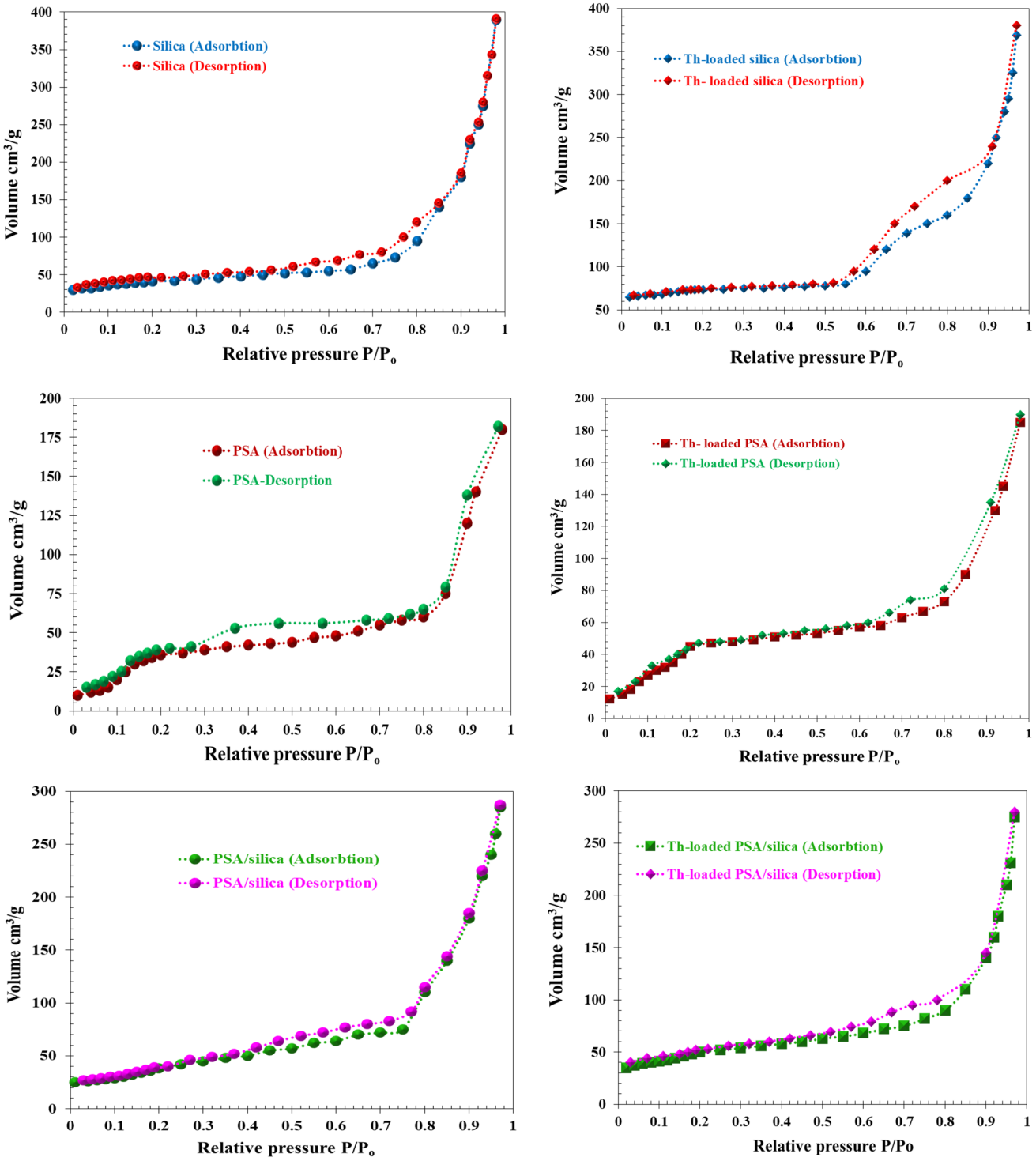

Fig. 4 N_2 adsorption/desorption isotherm of nano-silica, Th-loaded silica, PSA polymer, Th-loaded PSA, PSA/silica, and Th-loaded PSA/silica

3.2 Thorium ions adsorption

3.2.1 Solution pH

The influence of pH is a vital parameter for gaining a high adsorption capacity during the adsorption process. Thorium ionic species distribution in aqueous media at several pH values were exposed in Fig. 6a, which displayed that the hydrolyzation procedures of thorium ions were obviously depended on pH. According to Fig. 6a, at

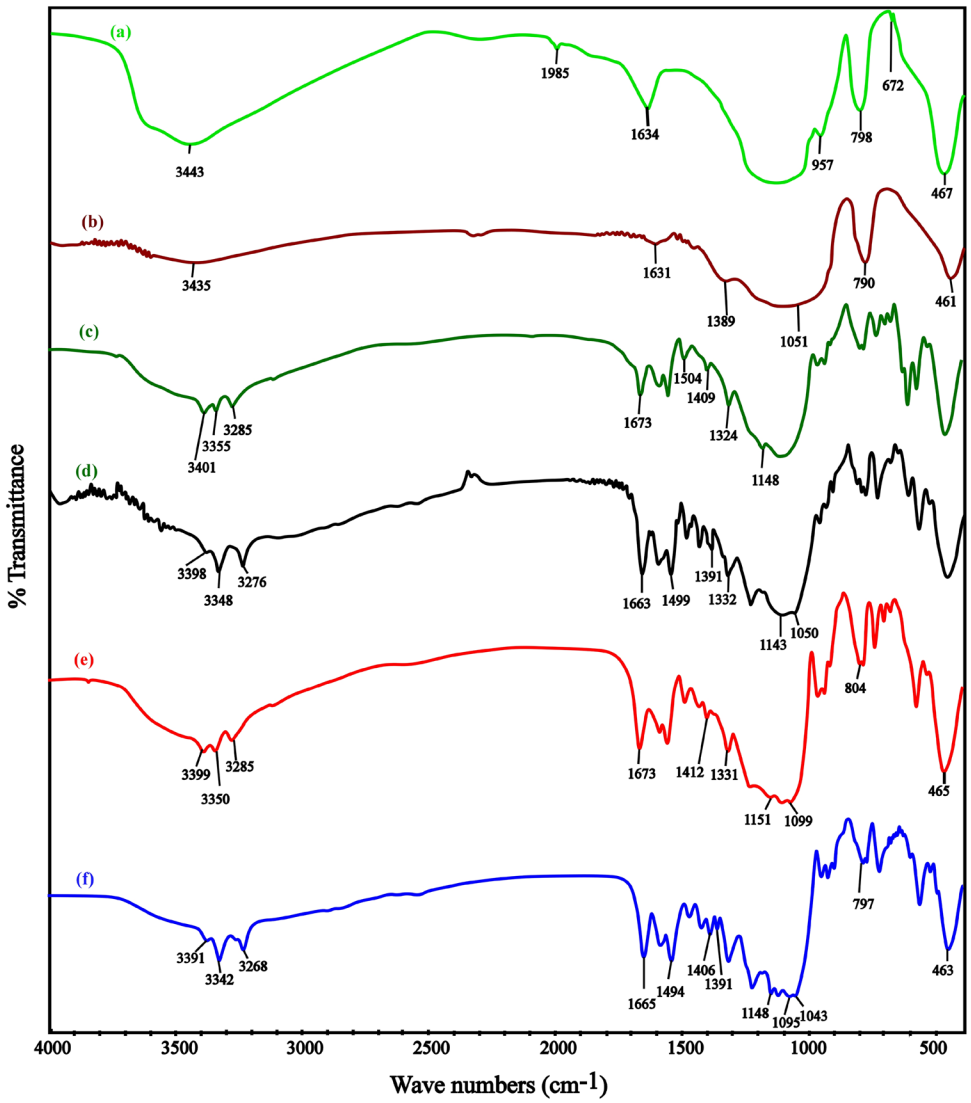

Fig. 5 FTIR spectra of of **a** nano-SiO_2, **b** Th-loaded SiO_2, **c** PSA, **d** Th-loaded PSA, **e** PSA/SiO_2, and **f** Th-loaded PSA/SiO_2

pH < 4.5, thorium ionic species distribution in the solution were mainly involved of positively charged species which are Th^{4+}, $Th_4(OH)_8^{8+}$, $Th_6(OH)_{15}^{9+}$, $Th(OH)^{3+}$, $Th(OH)_3^{+}$, and $Th(OH)_2^{2+}$. In addition, soluble thorium ions such as Th^{4+} were the dominant species in strongly acidic solution, while Th^{4+} tended to precipitate out as $Th(OH)_4$ at higher pH, which were remained compatible with the outcomes of earlier studies [48–50].

To assess the influence of solution pH on the Th(IV) adsorption capacity for nano-silica, PSA, and PSA/silica composites, the pH was examined in between pH1–7, and the outcomes were manifested in Fig. 6b. As a result that, Th(IV) adsorption was a remarkable dependent on the pH value due to pH influences the thorium ions solubility, and the ionization state of hydroxyl and sulfonamide groups holding on the three adsorbents surfaces. The adsorption capacities data displayed that with increasing pH values from 1 to 4, the amount of thorium ions adsorption capacities on the three adsorbents surfaces increased sharply due to the competition between H^+ and thorium cations for the capture of the binding sites. In other meanings, At pH < 4, thorium ions adsorption capacities on three adsorbents were low values because of the competing between the H^+ ions in the medium and thorium ions cationic species. Also, partial protonation of the hydroxyl and sulfonamide groups inhibiting the interactions between the adsorbents and thorium ions that could be the chief target for a small quantity of Th(IV) adsorption ability at pH < 4 [21]. At pH4, the surface positive charges on the adsorbents decreased and the thorium ions uptake capacities increased due to the increase of the attraction between the sorbate thorium cations species and adsorbents. After that, increasing pH more than 4, thorium ions adsorption capacities on the three adsorbents were decreased due to thorium ions was initially precipitated at pH > 4 according to the species distribution for thorium

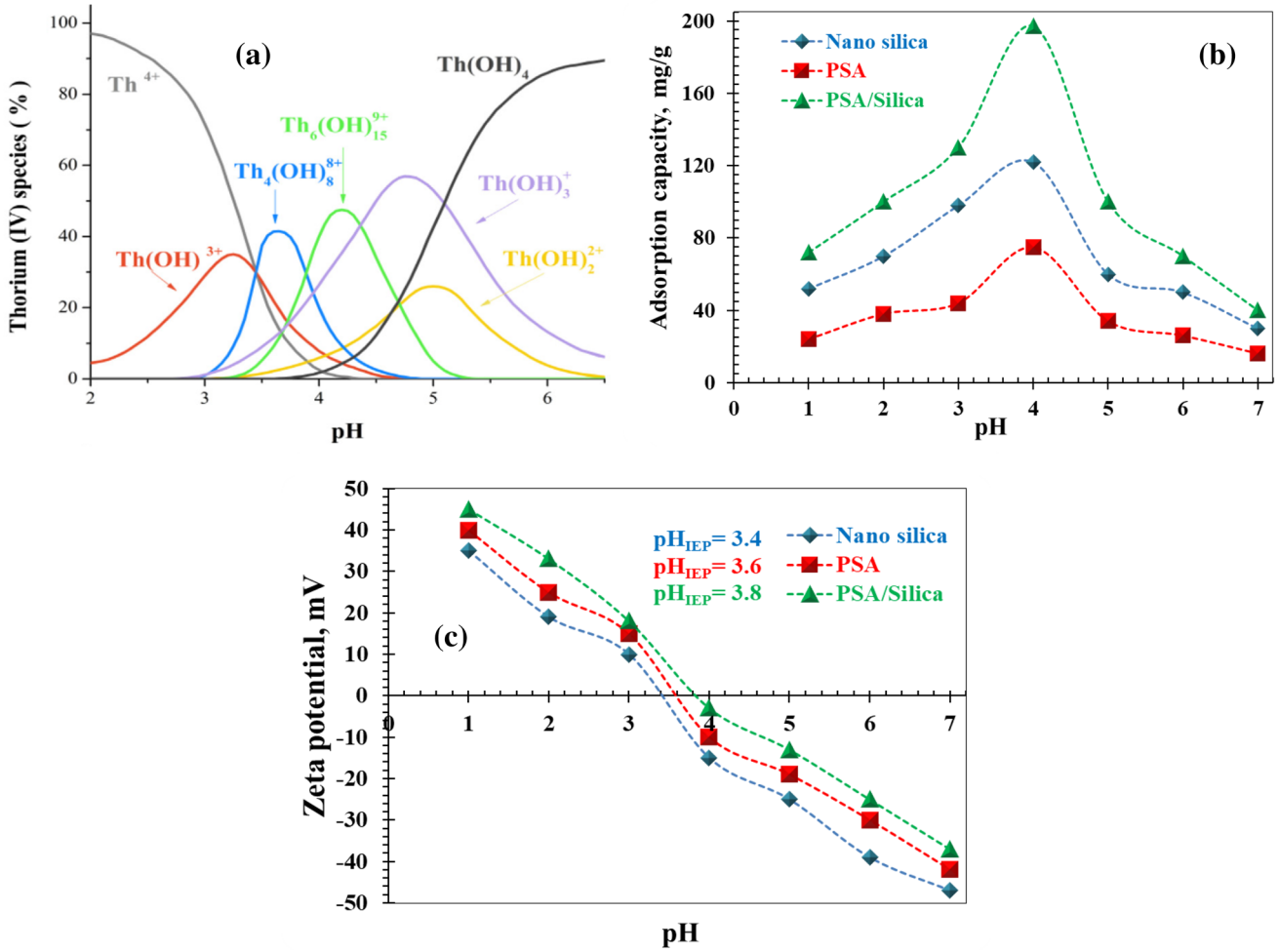

Fig. 6 **a** Thorium ions species distribution against pH (0.86 mmol/L thorium concentration at 298 K), **b** effect of pH on thorium adsorption on nano-silica, PSA, and PSA/silica (0.1 g adsorbent dose, 200 mg/L Th(IV) concentration, 100 mL solution, contact time 45 min, room temperature); and **c** zeta potential versus pH for nano-silica, PSA, and PSA/silica

ions hydrolysis. The zeta potential and pH influence were checked to pH values below 7 in the intended system. The zeta potential was demonstrated in Fig. 6c, and the results indicated that the pH values at the the isoelectric point (pH_{IEP}) were 3.2 (nano-silica), 3.6 (PSA), and 3.8 (PSA/silica). These were the three adsorbents had negatively charged meanwhile, the pH remained larger than the pH_{IEP} that might be convenient for thorium ions adsorption. Consequently, further adsorption studies were conducted at optimum pH4.

3.2.2 Ionic strength

To study the performance of thorium ions adsorption on nano-silica, poly sulfonamide, and PSA/silica more regularly and comprehensively, the influence of different background salts concentrations on thorium ions adsorption were examined. These salts comprised NaCl, KCl, and $MgCl_2$. Figure 7 showed the relationship between ionic strength and the thorium ions adsorption capacities onto nano-silica, poly sulfonamide, and PSA/silica for the three salts. The results displayed that the thorium ions adsorption capacities onto nano-silica, poly sulfonamide, and PSA/silica were not significantly affected by an increase in ionic strength from 0.0 to 0.1 mol/L, implying that at these experimental conditions, complexation between thorium ions and the adsorbents surfaces were performed [27]. According to these comments and the earlier mentioned data, thorium ions adsorption capacities were dependent on the solution pH rather than the ionic strength.

3.2.3 Contact time

Contact time of thorium ions solution and solid adsorbents is a key aspect in thorium ions adsorption because this aspect could represent the kinetics of interactions of

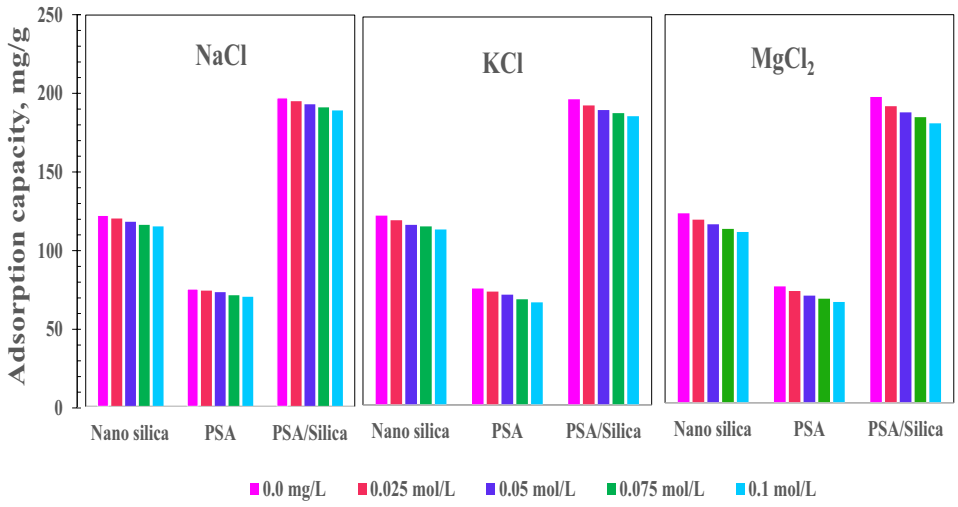

Fig. 7 Influence of ionic strength on thorium ions adsorption using nano-silica, PSA, and PSA/silica (pH: 4, 100 mL of 200 mg/L thorium concentration, 0.1 g adsorbent dose)

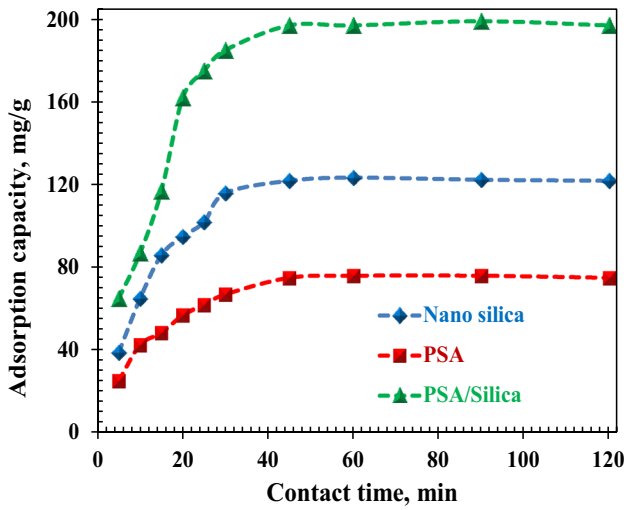

Fig. 8 Influence of contact time on thorium ions adsorption for nano-silica, PSA, and PSA/silica composites (pH4, 0.1 g adsorbent dose, room temperature, 200 mg/L Th(IV) concentration, 100 mL solution)

surface adsorbent with thorium ions. For this purpose, the influence of contact time on thorium ions adsorption onto nano-silica, PSA, and PSA/silica composites at room temperature was investigated at 200 mg/L thorium ions concentration (Fig. 8). The obtained data designated that the Th(IV) adsorption efficiencies increased from 39, 25, and 65 mg/g to 122, 75, and 197 mg/g of nano-silica, PSA, and PSA/silica composites, respectively with increasing contact time from 5 to 45 min. The adsorption capacities were fixed after 45 min for the three adsorbents, whereas extra increase of time had not influenced the thorium ions adsorption. Therefore, 45 min is the most sufficient contact time for all the equilibrium experiments.

Adsorption kinetic studies are crucial for the interpretation of the adsorption system, and they also provide valuable experimental and scientific data for thorium ions recovery. So, to examine thorium ions adsorption that depended on the reaction time and also determined the rate-controlling mechanism of thorium ions adsorption on nano-silica, PSA, and PSA/silica composites. The pseudo-first-order and pseudo-second-order kinetic mechanisms were employed for the evaluation of Th(IV) adsorption rate-controlling step. The pseudo-first-order kinetic mechanism believed that the adsorption system was controlled through physical interactions, while the mechanism proposed through a pseudo-second-order kinetic mechanism was that chemical adsorption happens throughout the complete adsorption process [51]. The pseudo-first-order mechanism was expressed in the following:

$$\log(q_e - q_t) = \log q_e - \frac{k_1 t}{2.303} \quad (3)$$

where the adsorption capacity of Th(IV) at equilibrium, and change time t (min) are q_e, and q_t, (mg/g) respectively, constant adsorption rate is k_1, (min^{-1}). Pseudo second-order mechanism expressed by the subsequent:

$$\frac{t}{q_t} = \frac{1}{k_2 q_e^2} + \frac{t}{q_e} \quad (4)$$

where k_2 is second-order adsorption constant (g/(mg min)). The plots of two kinetic models gained in Fig. 9. The kinetic parameters recorded in Table 1. Hence, the data illustrated that thorium ions adsorption on nano-silica, PSA, and PSA/silica composites followed the pseudo-second-order kinetic model owning to the excellent fit (R^2 more than 0.99) and approximately corresponding experimental capacities (122, 75, 197 mg/g) with the calculated capacities (129.87, 76.92, 204.08 mg/g) of this model. The

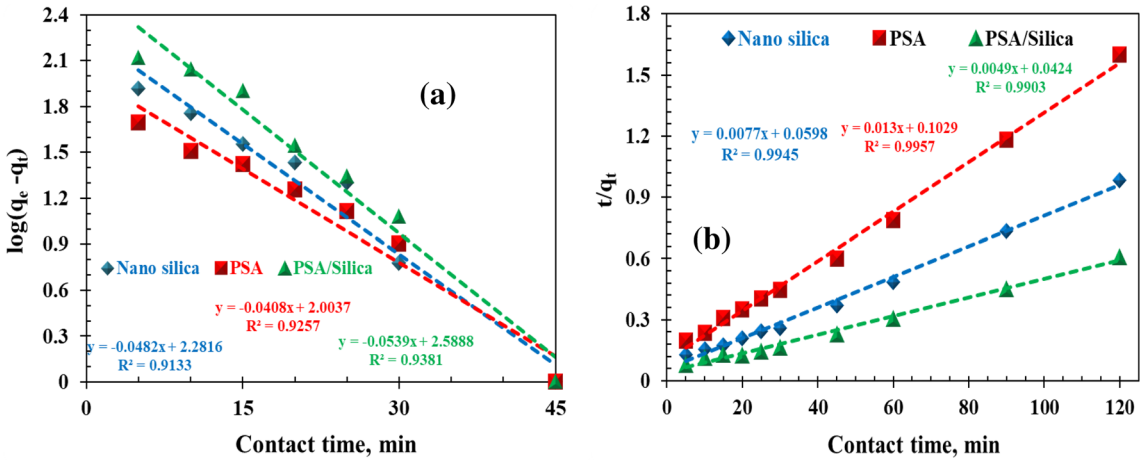

Fig. 9 Kinetic adsorption of Th(IV) on nano-silica, PSA, and PSA/silica composites, **a** Pseudo-first-order kinetic model, and **b** Pseudo-second-order kinetic model

Table 1 Kinetic parameters for Th(IV) adsorption on nano-silica, PSA, and PSA/silica composites

Kinetic models	Parameter	Nano-silica	PSA	PSA/silica
Pseudo-first-order	q_e (mg/g)	191.25	100.85	387.97
	k_1 (1/min)	0.111	0.094	0.124
	R^2	0.91	0.92	0.93
Pseudo-second-order	q_e (mg/g)	129.87	76.92	204.08
	k_2 (g/mg min)	9.91×10^{-4}	1.64×10^{-3}	0.47×10^{-3}
	R^2	0.99	0.99	0.99
Experimental capacity	q_{exp}	122	75	197

results obtained suggested that thorium ions adsorption on nano-silica, PSA, PSA/silica composites were controlled by chemisorption. Accordingly, the interaction between Th(IV) and adsorbents functional groups were correlated to valence bonds produced through sharing electrons might be observed in the adsorption process.

3.2.4 Adsorbent dose

The dose amount is a significant aspect of assessing the sorbent-metal ions at the equilibrium system. The effect of dose amount of nano-silica, PSA, and PSA/silica composites for Th(IV) adsorption was explored at the dose amount varied from 20 to 200 mg in 100 mL of the solution involving 200 mg/L thorium ions. Figure 10 reveals that the thorium ions adsorption capacities (q_e) had thus been fixed at 122, 75, 197 mg/g with the dose amount 120, 160, and 100 mg of nano-silica, PSA, and PSA/silica composites, respectively. The subsequent dose amounts increased, thorium ions adsorption capacities reduced because of the presence of silanol, C=O, –NH, and sulfone groups, which were binding thorium ions effectively by the strong and weak acid–base principle.

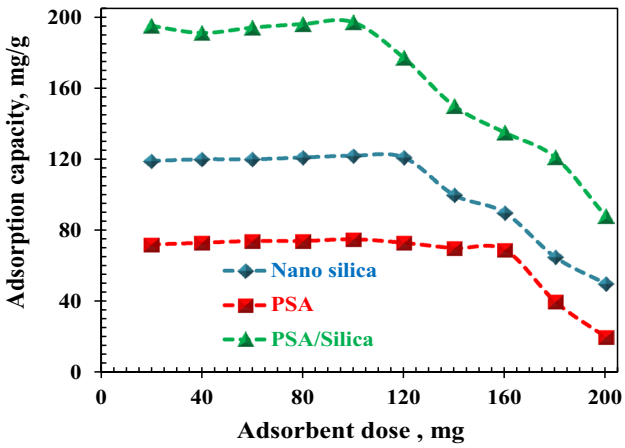

Fig. 10 Effect of dose amount of nano-silica, PSA, and PSA/silica composites on thorium ions adsorption (pH4, 45 min contact time, 200 mg/L Th(IV) concentration, 100 mL solution, room temperature)

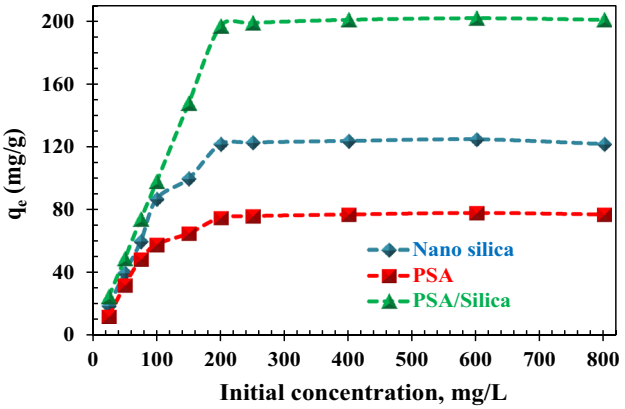

Fig. 11 Effect of the initial thorium ions concentration on the adsorption capacties for nano-silica, PSA, and PSA/silica composites (pH4, 45 min contact time, room temperature, 0.1 dose amount, 100 mL solution)

3.2.5 Initial Th(IV) concentration

The initial Th(IV) concentration directly affects the adsorption process and capacity. To study the relation of adsorption capacity versus metal ions concentration in the aqueous phase, it will help us to demonstrate the adsorption behavior. Therefore, the initial concentration of Th(IV) varied within the range 25–800 mg/L, and the other parameters were kept constant. From Fig. 11, the data indicated that Th(IV) concentration increased from 25 to 200 mg/L, the adsorption capacity increased with the metal ions concentration. At a 100 mg dose amount of nano-silica, PSA, and PSA/silica composites that had the limited active sites used when exceeded 200 mg/L Th(IV) were contained in the reaction system, and the adsorption capacities would overload the accessible binding sites at the three adsorbents. Under the present experimental conditions, the maximum adsorption capacities reached were 122, 75, and 197 mg/g of nano-silica, PSA, and PSA/silica composites.

Isotherms of adsorption illustrated whereby thorium ions that combined with nano-silica, PSA, and PSA/silica composites and it gave the required supplies for the strategy of the adsorption system for Th(IV) capture. Two models (Freundlich and Langmuir isotherms) were extensively realized here. Freundlich isotherm is a realistic model that had emerged in assuming a heterogeneous sarfaces by a non-uniform distribution of adsorption heat above the surface of nano-silica, PSA, and PSA/silica composites. It was extensively expressed as in the following Eq. 5 [52]:

$$\log q_e = \log K_f + \frac{1}{n} \log C_e \tag{5}$$

where K_f (mg/g) is Th(IV) adsorption equilibrium constant, n is Freundlich constant related to the intensity, C_e (mg/L) is equilibrium concentration of thorium ions, and q_e (mg/g) is Th(IV) equilibrium adsorption capacity on nano-silica, PSA, and PSA/silica composites. Langmuir isotherm assumed that the adsorption/binding of Th(IV) from solution was emerged on the homogenous surface through saturated monolayer adsorption on nano-silica, PSA, and PSA/silica surface at permanent adsorption energy. The Langmuir model signified in Eq. 6 [53]:

$$\frac{C_e}{q_e} = \frac{1}{q_m K_L} + \left(\frac{1}{q_m}\right) C_e \tag{6}$$

where K_L (L/mg) is Langmuir constant at equilibrium, and q_m is the maximum Th(IV) adsorption capacity (mg/g). Table 2 exhibited the results of adsorption isotherms of the two models. It was explained that the Freundlich model provided a pauper-fitting by tiny R^2 values 0.73, 0.67, and 0.63 for the practical results of nano-silica, PSA, and PSA/silica composites. Nonetheless, the practical data were effortlessly close-fitting to the Langmuir model, by great R^2 values (0.999) of nano-silica, PSA, and PSA/silica composites (Fig. 12). The estimated data characterized that the adsorption assemblies did not rely on the Freundlich model. On the contrary, the estimated adsorption capacities (q_m) for nano-silica, PSA, and PSA/silica composites with Langmuir isotherm were 121.95, 76.34, and 200.00 mg/g, respectively. These results labeled that Langmuir model was further fitted than Freundlich model for labeling the adsorption performance of the Th(IV) adsorption on nano-silica, PSA, and PSA/silica composites. These inferred a homogeneous arrangement of the surface active sites and monolayer surface of Th(IV) on nano-silica, PSA, and PSA/silica composites, correspondingly to the Langmuir model supposed the homogeneous surface.

A comparison of the maximum adsorption of Th(IV) onto various adsorbents in different experimental conditions was set in Table 3. As realized, the maximum adsorption of Th(IV) ions onto PSA/silica composite is better than that of the other reported adsorbents.

Table 2 Isotherm parameters of Th(IV) adsorption on nano-silica, PSA, and PSA/silica composites

Isotherm models	Parameter	Nano-silica	PSA	PSA/silica
Freundlich isotherm	K_f (mg/g)	28.07	19.97	73.08
	1/n (mg min/g)	0.274	0.239	0.203
	R^2	0.73	0.67	0.63
Langmuir isotherm	q_m (mg/g)	121.95	76.34	200.00
	K_L (L/mg)	0.134	0.114	0.77
	R^2	0.999	0.999	0.999
Experimental capacity	q_{exp}	122	75	197

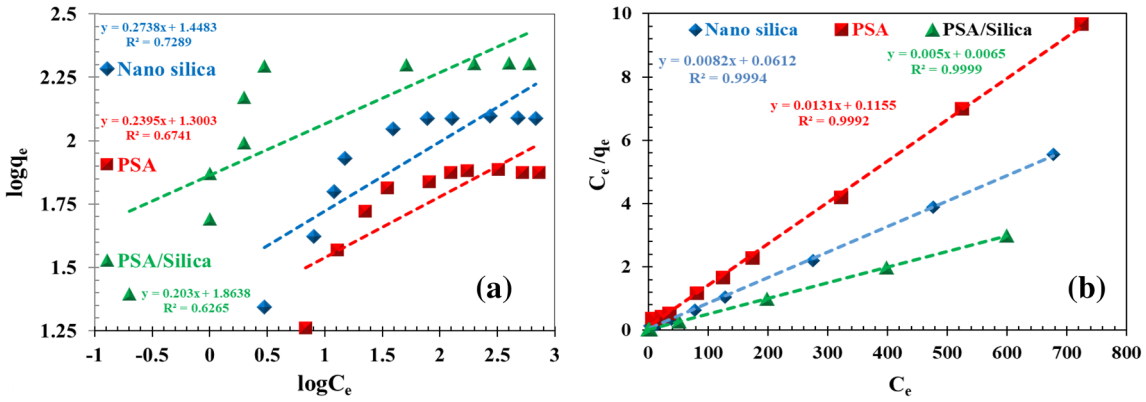

Fig. 12 Freundlich (**a**), and Langmuir (**b**) isotherm models of Th(IV) adsorption on nano-silica, PSA, and PSA/silica composites

Table 3 Comparison of the maximum adsorption capacity of Th(IV) ions by various adsorbents

Adsorbent	Uptake capacity (mg/g)	pH	Temperature (°C)	Adsorbent dose (g/L)	Contact time (min)	References
Magnetic talc/titanium oxide	54.5	3–4	25	2	120	[3]
1-(2-Pyridylazo)-2-naphthol/zeolite	9.28	4	25	3	45	[54]
chitosan/poly(acrylamide)	118.32	5	25	10	1440	[55]
P(4-vinyl pyridine) hydrogel	120.5	4	30	2.5	400	[56]
Monomodified b-cyclodextrin polyrotaxane	12.92	4	25	1	35	[28]
Poly(acrylamide)/apatite	294.64	4	40	10	1440	[57]
poly(methacrylic acid)-grafted chitosan/bentonite	110.5	5–6	30	2	180	[58]
N,N,N′,N′-tetraoctyldiglycolamide impregnated graphene aerogel	66.8	< 1	25	1	720	[59]
triethylene-tetramine modified magnetic chitosan	133.3	4	25	1	60	[60]
Poly sulfanamide/nano-silica	197	4	25	1	45	Present study

Table 4 Effect of temperature on thorium ions adsorption uptake for nano-silica, PSA, and PSA/silica composites (pH4, 45 min contact time, 0.1 g adsorbent dose, 200 mg/L Th(IV) concentration, 100 mL solution)

Temperature (K)	Th(IV) adsorption uptake (mg/g)		
	Nano-silica	PSA	PSA/Silica
298 K	122.0	75.0	197.0
303 K	121.8	74.7	196.8
308 K	121.5	74.3	196.6
313 K	121.1	74.1	196.3
318 K	120.8	73.9	196.1
323 K	120.5	73.6	195.9
328 K	120.3	73.4	195.6

3.2.6 Temperature

The adsorption capacity of metal ions for the adsorbate depends on the solution temperature. Hence, the influence of temperature on the amounts of nano-silica, PSA, and PSA/silica composites was explored at different temperatures (298–328 K). Table 4 illustrated that Th(IV) adsorption capacities reduced with the temperature increasing from 298 to 328 K. This incident could be due to the adsorption steps environment and the expanding mobility of thorium ions through a lower driving force. Another reason maybe because of the acceleration of several slow desorption steps on the adsorbent surface. Hence, the best adsorption temperature was ambient temperature.

From the practical results, the free energy $\Delta G°$ (kJ/mol), enthalpy $\Delta H°$ (kJ/mol), and entropy $\Delta S°$ (kJ/mol K) of Th(IV) adsorption from acidic solution on nano-silica, PSA, and PSA/silica composites were evaluated using the change of absolute temperature T (K) and the thermodynamic equilibrium constant (K_e^0, L/g) that estimated from Eq. 7. The thermodynamic factors of the adsorption organizations established by Vant' Hoff equation by

thermodynamic equilibrium constants (K_e^0, L/g) that were gotten at 298–328 K as the following Eq. (7) [61, 62].

$$K_e^0 = \frac{1000 \cdot K_g \cdot (\text{molecular weight of adsorbate})[\text{adsorbate}]^0}{\gamma} \quad (7)$$

where γ is the activity coefficient (dimensionless), $[\text{Adsorbate}]^0$ is the standard concentration of the thorium ions (1 mol/L), and K_e^0 is the thermodynamic equilibrium constant that is dimensionless that evaluated via converting the units of K_g (Langmuir equilibrium constant (K_L, L/mg) used since it was the supreme isotherm model) to L/mol. The modification achieved by multiplication of the Langmuir equilibrium constant (L/mg) values by 1000, to vary L/mg to L/g and therefore the creation of the multiplication of this data by the molecular weight of the thorium ions (g/mol) multiplied by the unitary standard concentration of thorium ions (1 mol/L) and creation of the division by activity coefficient (dimensionless). According to this evaluation, it was assumed that the solution of thorium ions is much diluted to considered that the activity coefficient was unitary. The factor K_e^0 turns into dimensionless after creation of these evaluations. These parameters assessed from the next Van't Hoff equations.

$$\log K_e^0 = \frac{\Delta S^\circ}{2.303R} - \frac{\Delta H^\circ}{2.303RT} \quad (8)$$

$$\Delta G^\circ = \Delta H^\circ - T\Delta S^\circ \quad (9)$$

R (8.314 J/mol K) is a universal gas constant. The ΔH° and ΔS° were predictable via the slope and intercept of linear plots of $\log K_e^0$ versus 1/T (Fig. 13). The ΔG°, ΔH°, and ΔS° values were recorded in Table 5.

From the achieved data, the negative ΔG° values exhibited that adsorption systems at all temperatures were achievability spontaneous in nature. Moreover, the ΔG° of the interactions permitted that the adsorption performances were required for the formation of the Th(IV) electrostatic interaction from acidic solution and the three adsorbents. The negative ΔH° values set exothermic of adsorption systems. Additionally, the positive ΔS° values initiated the feasibility and randomness of the adsorption systems for Th(IV) on nano-silica, PSA, and PSA/silica composites.

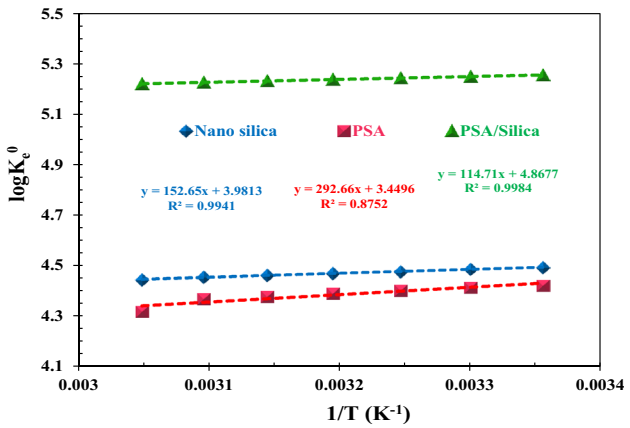

Fig. 13 Plot of log K_e^0 vs. 1/T of Th(IV) adsorption on nano-silica, PSA, and PSA/silica composites

3.2.7 Coexisting ions

Coexisting ions influence on the adsorption evolutions of target thorium ions through competition for the limited active sites of nano-silica, PSA, and PSA/silica. The effect of coexisting cations (as U(VI), Fe(III), Cr(II), Pb(II), Mg(II), Mn(II), and Sr(II)) that existed in nuclear waste of Nuclear Materials Authority, Egypt on thorium ions adsorption were investigated at the binary cationic system, and the data demonstrated in Fig. 14. At binary systems, a 1:1 concentration ratio was used to specify the competitive effect of individual metal ion on Th(IV) adsorption by varying the coexisting concentration cations from 25 to 200 mg/L. Th(IV) adsorption capacities in all of the binary systems were smaller than that in single thorium ions system. This

Table 5 Thermodynamic parameters of Th(IV) adsorption on nano-silica, PSA, and PSA/silica composites

T (K)	Langmuir constant (L/mg)			ΔG° (KJ/mol)		
	Nano-silica	PSA	PSA/Silica	Nano-silica	PSA	PSA/Silica
298	0.134	0.114	0.77	− 25.571	− 25.268	− 29.910
303	0.132	0.112	0.76	− 25.951	− 25.598	− 30.375
308	0.129	0.109	0.75	− 26.331	− 25.928	− 30.840
313	0.127	0.106	0.74	− 26.711	− 26.258	− 31.305
318	0.125	0.103	0.73	− 27.091	− 26.588	− 31.770
323	0.123	0.101	0.72	− 27.471	− 26.918	− 32.235
328	0.12	0.09	0.71	− 27.851	− 27.248	− 32.700
ΔH° (kJ/mol)				− 2.923	− 5.6	− 2.196
ΔS° (kJ/mol K)				0.076	0.066	0.093

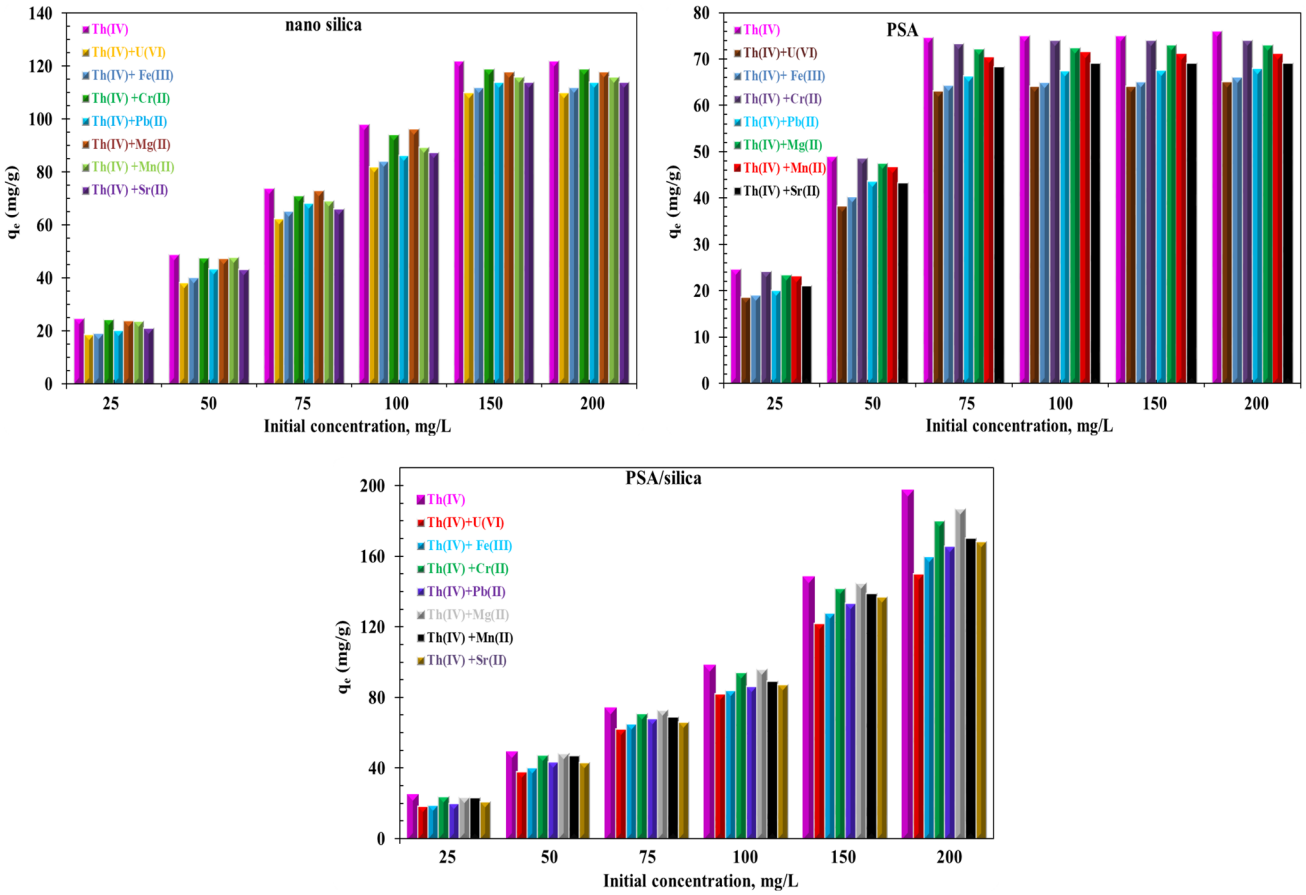

Fig. 14 Influence of coexisting ions on Th(IV) adsorption capacities of nano-silica, PSA, and PSA/silica composites (1:1 concentration ratio, pH4, 45 min contact time, 0.1 g adsorbent dose, 100 mL solution)

aspect was associated with many parameters such as the metal ions electronegativity, ionic potential, and competition between several cations to fill active sites of solid adsorbent. The attained data in binary systems (Fig. 14) displayed that Cr(II), Mg(1I), and Mn(II) did not produce a detectable influence on thorium ions uptake up to 50 mg/L concentration, however extra cations concentration had an inadequate inhibitory effect. At concentrations more than 50 mg/L, all the studied cations reduced significantly the Th(IV) adsorption. Few drops of 20 mM/L sodium tartrate and citrate, mixture solution used during the thorium ions adsorption processes to avoid the passive impact of the studied coexisting ions. The results of competitive adsorption in binary systems presented that the inhibitory influence of the studied metal ions on Th(IV) adsorption by nano-silica, PSA, and PSA/silica increased in order of U(VI) > Fe(III) > Pb(II) > Sr(II) > Mg(II) > Mn(II) > Cr(II).

3.3 Desorption and reusability

Th(IV)-loaded adsorbents were regenerated using HCl solution. Various concentrations of HCl ranging from 0.01 to 0.15 M/L were investigated for elution of adsorbed Th(IV) on nano-silica, PSA, and PSA/silica composites. Thorium ions desorption efficiencies from Th-loaded nano-silica, Th-loaded PSA, and Th-loaded PSA/silica were increased to 98.1, 97.9, and 99.1%, respectively, with increasing the HCl concentration from 0.01 to 0.1 M/L

Table 6 Effect of HCl concentration on the thorium ions desorption efficiencies from Th-loaded silica, Th-loaded PSA, and Th-loaded PSA/silica (2 g thorium ions loaded adsorbent, 50 mL solution, 60 min desorption time, room temperature)

HCl (M/L)	Desorption efficiency (%)		
	Nano-silica	PSA	PSA/Silica
0.01	55.2	52.8	57.8
0.03	65.2	62.6	68.3
0.5	72.3	70.11	74.7
0.08	81.4	80.1	84.8
0.1	98.1	97.9	99.1
0.12	98.5	98.1	99.1
0.15	98.3	98.2	99.2

(Table 6). Therefore, the best optimum concentration of HCl was determined as 0.1 M/L according to economical process for desorption processes. After adsorption, the Th(IV)-loaded adsorbents were desorbed in 0.1 M/L HCl solution, and the mixture was shaken 60 min contact time. After that, the solid adsorbents were washed to be neutral (pH7) by deionized water and then dried at 45 °C under vacuum drying oven and reused for the following experiments.

According to the previous study, the regeneration and reusability of nano-silica, PSA, and PSA/silica composites were significant parameters for evaluating their attainable practical industrial applications. Thorium ions loaded on the prepared adsorbents were submerged in 0.1 M/L HCl solution for regeneration. In Fig. 15, it was clear that Th(IV) adsorption–desorption efficiencies on nano-silica, PSA, and PSA/silica composites slowly reduced with following number of cycles. The regenerated and reused of the prepared adsorbents were done by 50 mL of a slightly alkaline solution, to remove any entrained chloride ions from the nano-silica, PSA, and PSA/silica prior to the recycle into the thorium ions adsorption system. At six cycles of reusability of nano-silica, PSA, and PSA/silica, the desorption efficiencies re-reached up to 81.2, 83.8, and 84.7% of the initial desorption efficiencies, respectively. Thus, it could be decided that PSA/silica with long-time constancy was admitted as a brilliant reusable adsorbent for high efficient Th(IV) removal.

3.4 Case study

Chemical analysis of the three nuclear waste solutions from the Nuclear Materials Authority reveals that they mainly contained Sr^{2+}, Mg^{2+}, Fe^{3+}, Mn^{2+}, SO_4^{2-}, Th^{4+}, UO_2^{2+}, Cr^{2+}, and Pb^{2+}. Thorium ions adsorption processes from 10 L the separate three waste solutions (a, b, and c) that have Th(IV) ions concentration of 103, 165, and 195 mg/L (Table 7) were carried out under the above optimum adsorption conditions using 10 g of PSA/silica adsorbent at 45 min contact time. Few drops of 20 mM/L sodium tartrate and citrate mixture solution utilized to avoid the adverse effect of the interfering ions. After equilibrium, the solutions were filtrated and analyzed for measuring Th(IV) ions concentration. It was observed that approximately all Th(IV) ions were adsorbed by PSA/silica, and the thorium ions concentration in the effluent was 2, 5, 6 mg/L for the three waste solutions (a, b, and c), It wasreflected a high adsorption efficiency of thorium ions (99.1%). The data exhibited that PSA/silica was wholly effective for Th(IV) ions adsorption from the waste samples. The loaded Th(IV) ions could be desorbed by contacting the 10 g Th-loaded PSA/silica with 250 mL of 0.1 M/L HCl for 60 min contact time. The achieved results revealed that nearly 98.2% of Th(IV) were desorbed from the loaded PSA/silica. These conclusions imply that the applied adsorption design is extremely selective for the trapping/adsorption of thorium ions really from waste solutions.

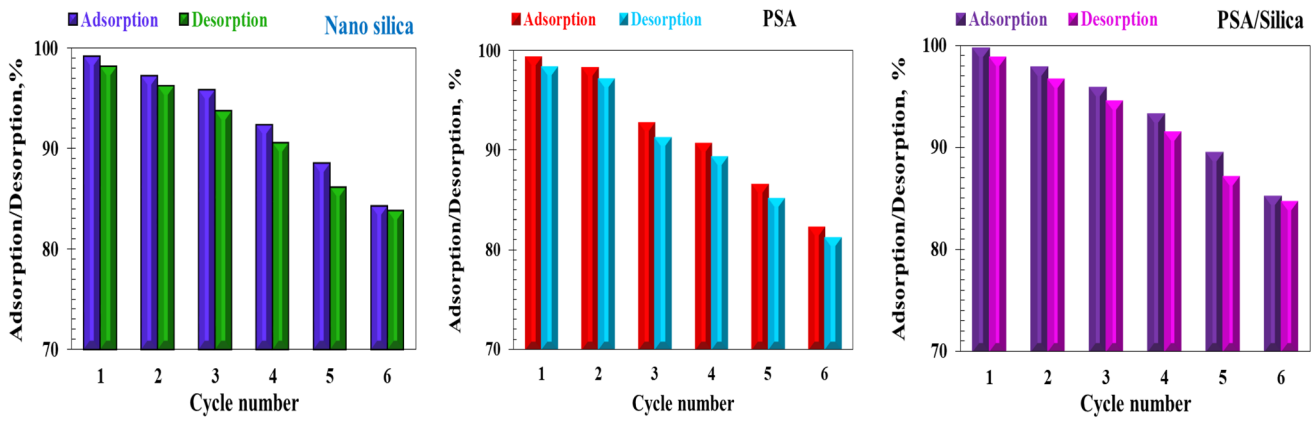

Fig. 15 The adsorbed and desorbed of thorium ions efficiency as adsorption–desorption cycle function

Table 7 The chemical constitutions (mg/L) of the three waste solutions

Sample	pH	Sr^{2+}	Mg^{2+}	Fe^{3+}	Mn^{2+}	SO_4^{2-}	Th^{4+}	UO_2^{2+}	Cr^{2+}	Pb^{2+}
a	4.1	55	332	2402	178	1343	103	67	90	33
b	3.8	128	242	2483	266	1762	165	103	77	85
c	3.9	161	291	2297	322	1512	195	164	36	99

4 Conclusion

In the actual work, a series of adsorption experiments of thorium ions were applied to attain the optimum adsorption parameters on the prepared composites that are nano-silica, PSA, and PSA/silica. The optimized conditions of the adsorption processes achieved using 100 mL of 200 mg/L Th(IV) stirred with 0.1 g of individual adsorbents at pH4 for 45 min contact time at room temperature. Under these conditions, the maximum uptake capacities of the nano-silica, PSA, and PSA/silica composites attained 122, 75, and 197 mg/g at 298 K. Furthermore, the kinetic data established to fit well through pseudo-second-order mechanism that was the best for clarifying the adsorption reaction. Also, Langmuir adsorption isotherm was more appropriate for illustrative the adsorption processes for the three adsorbents. Besides the studied thermodynamic parameters were resulted negative values of ΔH representing an exothermic reaction and positive values of ΔS indicating random behavior for Th(IV) adsorption, while the negative values of ΔG designated a spontaneous reaction of Th(IV) adsorption. The maximum Th(IV) desorption from the loaded adsorbents could be easily performed using 0.1 M/L HCl. Practical application studies exhibited that PSA/silica was effectively used as efficient thorium ions removal from the waste solutions. Hence, PSA/silica composite has the possibility been for working in the thorium ions recovery.

Compliance with ethical standards

Conflict of interest The authors declare that they have no conflict of interest.

References

1. Liu P, Qi W, Du Y-F, Li Z, Wang J, Bi J-J, Wu W-S (2014) Adsorption of thorium(IV) on magnetic multi-walled carbon nanotubes. Sci China Chem 57:1483–1490
2. Shiri-Yekta Z, Yaftian MR, Nilchi A (2013) Silica nanoparticles modified with a Schiff base ligand: an efficient adsorbent for Th(IV), U(VI), and Eu(III) ions. Korean J Chem Eng 30(8):1644–1651
3. Morsy AMA (2017) Performance of magnetic talc titanium oxide composite for thorium ions adsorption from acidic solution. Environ Technol Innov 8:399–410
4. Borai EH, Ahmed IM, Shahr El-Din AM, Abd ElGhany MS (2018) Development of selective separation method for thorium and rare earth elements from monazite. J Radioanal Nucl Chem 316(2):443–450
5. Chen Y, Wei Y, He L, Tang F (2016) Separation of thorium and uranium in nitric acid solution using silica based anion exchange resin. J Chromatog A 1466:37–41
6. Shagalov VV, Sobolev VI, Turinskaya MV, Malin AV (2016) Research of the thorium purification at monazite refinement processes. In: Iop conference series: materials science and engineering vol 135, pp 012041-5
7. Pawar RR, Suryavanshi VJ, Salunkhe ST, Patil SS, Mulik GN (2017) Liquid–liquid extraction of thorium(IV) with N-n-heptylaniline from acid media. J Radioanal Nucl Chem 311(1):419–426
8. Cheira MF, Orabi AS, Atia BM, Hassan SM (2018) Solvent extraction and separation of thorium(IV) from chloride media by a Schiff base. J Sol Chem 47(4):611–633
9. Cheira MF, Orabi AS, Hassanin MA, Hassan SM (2018) Solvent extraction of thorium(IV) from chloride solution using schiff base and its application for spectrophotometric determination. Chem Data Coll 13–14:84–103
10. Ilaiyaraja P, Deb AKS, Sivasubramanian K, Ponraju D, Venkatraman B (2013) Removal of thorium from aqueous solution by adsorption using PAMAM dendron-functionalized styrene divinylbenzene. J Radioanal Nucl Chem 297(1):59–69
11. Prasetyo E, Toyoda K (2017) Solid phase extraction of thorium and uranium and their separation from lanthanides using humic acid silica gel as a low-cost adsorbent. J Eng Techn Sci 49(4):508–519
12. Shiri-Yekta Z (2019) Removal of Th(IV) ion from wastewater using a proper Schiff base impregnated onto Amberlite XAD-4. Part Sci Technol 37(7):1–11
13. Rojo I, Seco F, Rovira M, Giménez J, Cervantes G, Martí V, Pablo J (2009) Thorium sorption onto magnetite and ferrihydrite in acidic conditions. J Nucl Mater 285:474–478
14. Bursali EA, Merdivan M, Yurdakoc M (2010) Preconcentration of uranium(VI) and thorium(IV) from aqueous solutions using low-cost abundantly available sorbent. J Radioanal Nucl Chem 283:471–476
15. Qian L-J, Zhao J-N, Hu P-Z, Geng Y-X, Wu W-S (2010) Effect of pH, fulvic acid and temperature on sorption of Th(IV) on zirconium oxophosphate. J Radioanal Nucl Chem 283:653–660
16. Duan G, Zhong Q, Bi L, Yang L, Liu T, Shi X, Wu W (2017) The poly(acrylonitrule-co-acrylic acid)-graft-β-cyclodextrin hydrogel for thorium(IV) adsorption. Polymers 9(6):1–14
17. Abbasizadeh S, Keshtkar AR, Mousavian MA (2013) Preparation of a novel electrospun polyvinyl alcohol/titanium oxide nanofiber adsorbent modified with mercapto groups for uranium(VI) and thorium(IV) removal from aqueous solution. Chem Eng J 220:161–171
18. Wu S, Li F, Wang H, Fu L, Zhang B, Li G (2010) Effects of poly (vinyl alcohol) (PVA) content on preparation of novel thiol-functionalized mesoporous PVA/SiO_2 composite nanofiber membranes and their application for adsorption of heavy metal ions from aqueous solution. Polymer 51:6203–6211
19. Kaynar ÜH, Şabikoğlu I, Kaynar SÇ, Eral M (2016) Modeling of thorium(IV) ions adsorption onto a novel adsorbent material silicon dioxide nano-balls using response surface methodology. Appl Rad Iso 115:280–288
20. Kaynar ÜH, Ayvacıklı M, Hiçsönmez Ü, Kaynar SÇ (2015) Removal of thorium (IV) ions from aqueous solution by a novel nanoporous ZnO: isotherms, kinetic and thermodynamic studies. J Environ Radioact 150:145–151
21. Nilchi A, Dehaghan TS, Garmarodi SR (2013) Kinetics, isotherm and thermodynamics for uranium and thorium ions adsorption from aqueous solutions by crystalline tin oxide nanoparticles. Desalination 321:67–71
22. Malekynejad A, Sepehrian H, Manoochehri M (2013) Adsorption of thorium from aqueous solution using nanoporous adsorbents: effect of contact time, pH, initial concentration, and temperature. Particulate Sci Technol 31:372–378
23. Nosach LV, Voronin EF, Pakhlov EM, Charmas B, Skubiszewska-Zięba J, Skwarek E, Janusz W, Gun'ko VM (2017) Nano-particulate structures with glucose-derived char and compacted fumed silica in gaseous and aqueous media. Chapter 56, Nanophysics,

Nanomaterials, Interface Studies, and Applications Springer Proceedings in Physics 195:729–742
24. Andriyko LS, Zarko VI, Gun'ko VM, Marynin AI, Olishevskiy VV, Skwarek E, Janusz W (2015) Electrical and physical characteristics of silica nanoparticles in aqueous media affected by cations Na^+, Ba^{2+} and Al^{3+}. Ads Sci Technol 33(68):601–608
25. Goncharuk O, Bogatyrov V, Kazakova O, Galaburda M, Oranska O, Skwarek E, Waniak-Nowicka H, Janusz W, Gun'ko V (2019) Silica-supported Ni_xO_y, Zn_xO_y and Mn_xO_y nanocomposites: physicochemical characteristics and interactions with water and n-decane. Bull Mater Sci 42:243
26. Souderjani EZ, Keshtkar AR, Mousavian MA (2017) Application of response surface methodology for thorium(IV) removal using Amberlite IR-120 and IRA-400: ion exchange equilibrium and kinetics. J Part Sci Techn 3:101–112
27. Duan GJ, Zhong QQ, Bi L, Yang L, Liu TH, Shi XN (2017) The poly(acrylonitrule co-acrylic acid)-graft-b-cyclodextrin hydrogel for thorium(IV) adsorption. Polymers 9:201–211
28. Liu H, Qi C, Feng Z, Lei L, Deng S (2017) Adsorption of trace thorium(IV) from aqueous solution by monomodified b-cyclodextrin polyrotaxane using response surface methodology (RSM). J Radioanal Nucl Chem 314:1607–1618
29. Keshtkar AR, Irani M, Moosavian MA (2013) Comparative study on PVA/silica membrane functionalized with mercapto and amine groups for adsorption of Cu(II) from aqueous solutions. J Taiwan Inst Chem Eng 44:279–286
30. Eichhlorn S, Dufresne A, Aranguren M, Marcovich N, Capadona JR, Rowan SJ, Weder C, Thielemans W, Roman M, Renneckar S, Gindl W, Veigel S, Keckes J, Yano H, Abe K, Nogi M, Nakagaito AN, Mangalam A, Simonsen J, Benight AS, Bismarck A, Berglund LA, Peijs T (2010) Review, current international research into cellulose nanofibers and nanocomposites. J Mater Sci 45:1–33
31. Saheb D, Jog J (1999) Nature fiber polymer composite: a review. Adv Polym Technol 18:351–363
32. Zhang J, Liu Z, Kong Q, Zhang C, Pang S, Yue L, Wang X, Yao J, Cui G (2013) Renewable and superior thermal-resistant cellulose-based composite nonwoven as lithium-ion battery separator. ACS Appl Mater Interfaces 5:128–134
33. Zhang J, Yue L, Kong Q, Liu Z, Zhou X, Zhang C, Pang S, Wang X, Yao J, Cui G (2013) A heat-resistant silica nanoparticle enhanced polysulfamide nonwoven separator for high-performance lithium-ion battery. J Electrochem Soc 160:A769–A774
34. Marczenko Z, Balcerzak M (2000) Separation, preconcentration, and spectrophotometry in inorganic analysis. Elsevier Science B.V, Amsterdam the Netherlands, p 521p
35. Bao M, Zhu G, Wang L, Wang M, Gao C (2013) Preparation of monodispersed spherical mesoporous nanosilica–polyamide thin film composite reverse osmosis membranes via interfacial polymerization. Desalination 309:261–266
36. Li L, Wei-tao W, Chang-fa X (2010) Preparation and Characterization of Polysulfonamide Statistical Copolymers from Three Aromatic Diamines. J Shanghai Jiaotong Univ (Sci) 15(1):114–118
37. Zhang X, Tang X, Wang R, Wang R, Yan X, Shi M (2018) The fire retardant properties and pyrolysis mechanism of polysulfonamide (PSA) fibers. Textile Res J 88(11):1299–1307
38. Chan W, Lam-Leunc SY, Ding CNJ, Xi S (1995) Synthesis and characterization of poly(amide sulfonamide)s (PASAs). Polymer Chem 33(15):2525–2531
39. Tang Z, Xu W, Jia Q (2010) Preparation of the polysulfonamide/titania composites. J Shanghai Univ (English Edition) 14:460–463
40. Salimi F, Tahmasobi K, Karami C, Jahangiri A (2017) Preparation of modified nano-SiO_2 by bismuth and iron as a novel remover of methylene blue from water solution. J Mex Chem Soc 61(3):250–259
41. Cullity BD, Stock SR (2001) Elements of X-ray Diffraction, 3rd edn. Prentice-Hall, New York
42. Douglas B, Ho S (2006) Crystal Structures of Silica and Metal Silicates. Structure and Chemistry of Crystalline Solids. Springer, New York, NY, pp 233–278
43. Abou Rida M, Harb F (2014) Synthesis and characterization of amorphous silica nanoparticles from aqueous silicates using cationic surfactants. J Met Mater Miner 24(1):37–42
44. Guo Q, Yang G, Huang Cao DW, Ge L, Li L (2018) Synthesis and characterization of spherical silica nanoparticles by modified Stöber process assisted by slow-hydrolysis catalyst. Coll Polymer Sci 296:379–384
45. Lu P, Hsieh Y (2012) Highly pure amorphous silica nano-disks from rice straw. Powder Technol 225:149–155
46. Liu L, Wang D, Xu T, Jia L, Ding F, Zhang S (2013) Synthesis and characterization of wholly aromatic poly (amide-sulfonamide)s by solution polycondensation. Adv Mat Res 821–822:949–952
47. Pool JA, Scott BL, Kiplinger JL (2005) A new mode of reactivity for pyridine N–oxide: C-H activation with uranium(IV) and thorium(IV) bis(alkyl) complexes. J Am Chem Soc 127:1338–1339
48. Baybaş D, Ulusoy U (2011) The use of polyacrylamide-aluminosilicate composites for thorium adsorption. Appl Clay Sci 51:138–146
49. Huang Y, Hu Y, Chen L, Yang T, Huang H, Shi R, Lu P, Zhong C (2018) Selective biosorption of thorium (IV) from aqueous solutions by ginkgo leaf. PLoS ONE 13:e0193659–e0193683
50. Ding H, Zhang X, Yang H, Luo X, Lin X (2019) Highly efficient extraction of thorium from aqueous solution by fungal mycelium-based microspheres fabricated via immobilization. Chem Eng J 368:37–50
51. Cheira MF, Mira HI, Sakr AK, Mohamed SA (2019) Adsorption of U(VI) from acid solution on a low-cost sorbent: equilibrium, kinetic, and thermodynamic assessments. Nucl Sci Technol 30:156
52. Yang Z, Chen G, Weng H, Shen W, Huang Z, Lin M (2018) Efficient and selective separation of U(VI) and Th(IV) from rare earths using functionalized hierarchically mesoporous silica. J Mater Sci 53(5):3398–3416
53. Cheira MF, Atia BM, Kouraim MN (2017) Uranium(VI) recovery from acidic leach liquor by Ambersep 920U SO_4 resin: kinetic, equilibrium and thermodynamic studies. J Rad Res Appl Sci 10:307–319
54. Kaygun AK, Akyil S (2007) Study of the behaviour of thorium adsorption on PAN/zeolite composite adsorbent. J Hazard Mater 147:357–362
55. Akkaya R, Ulusoy U (2008) Adsorptive features of chitosan entrapped in polyacrylamide hydrogel for Pb^{2+}, UO_2^{2+}, and Th^{4+}. J Hazard Mater 151:380–388
56. Ozay O, Ekici S, Aktas N, Sahiner N (2011) P(4-vinyl pyridine) hydrogel use for the removal of UO22 + and Th4 + from aqueous environments. J Environ Manag 92:3121–3129
57. Ulusoy U, Akkaya R (2009) Adsorptive features of polyacrylamide–apatite composite for Pb^{2+}, UO_2^{2+}, and Th^{4+}. J Hazard Mater 163:98–108
58. Anirudhan TS, Rijith S, Tharun A (2010) Adsorptive removal of thorium(IV) from aqueous solutions using poly(methacrylic acid)-grafted chitosan/bentonite composite matrix: process design and equilibrium studies. Coll Surf A: Physicochem Eng Aspects 368:13–22
59. Chen M, Li Z, Geng Y, Zhao H, He S, Li Q, Zhang L (2018) Adsorption behavior of thorium on N, N, N′, N′-tetraoctyldiglycolamide (TODGA) impregnated graphene aerogel. Talanta 181:311–317
60. Xu J, Zhou L, Jia Y, Liu Z, Adesina AA (2015) Adsorption of thorium (IV) ions from aqueous solution by magnetic chitosan resins modified with triethylene-tetramine. J Radioanal Nucl Chem 303:347–356

61. Cheira MF (2015) Synthesis of pyridylazo resorcinol–functionalized Amberlite XAD-16 and its characteristics for uranium recovery. J Environ Chem Eng 3:642–652
62. Lima EC, Hosseini-Bandegharaei A, Moreno-Piraján JC, Anastopoulos I (2019) A critical review of the estimation of the thermodynamic parameters on adsorption equilibria. Wrong use of equilibrium constant in the Van't Hoof equation for calculation of thermodynamic parameters of adsorption. J Mol Liq 273:425–434